Journal of the Energy Institute 106 (2023) 101130

Contents lists available at ScienceDirect

Journal of the Energy Institute

journal homepage: www.elsevier.com/locate/joei

Comparative analysis of ammonia combustion for domestic applications

Bahamin Bazooyar *, George Coomson, Vasilije Manovic, Seyed Ali Nabavi **

Centre for Climate and Environmental Protection, Cranfield University, Bedford, Bedfordshire, MK43 0AL, UK

ARTICLE INFO

Keywords:
Ammonia
Ammonia combustion
Boiler
Gas turbine
Computational fluid dynamics
Alternative fuel

ABSTRACT

This article explores whether ammonia is a reliable fuel for heat and electricity generation in domestic applications. First, the ammonia combustion characteristics, including adiabatic flame temperature, ignition delay time, and laminar flame speed are analysed and compared with the conventional fuels such as natural gas, dimethyl ether, hydrogen, and syngas, under 12 kWe turbine and 45kWth boiler conditions. Furthermore, the combustion of ammonia at a conventional boiler and turbine combustor was numerically modelled, analysed, and compared with the available fuels. The finding demonstrates that ammonia provides inferior combustion characteristics in combustion heat releases, stability region, and ignition characteristics. The ammonia combustion characteristics including, laminar flame speed and ignition delay time, were comparable to those of methane. The flame temperature and exhaust gas composition of ammonia are rather different than those of methane which may vary the heat transfer during the operation of gas turbines and boilers. The combustion of ammonia in boilers may produce the required heat for heating purposes; however, it needs further modification to achieve better NO_X control. In a gas turbine, on the other hand, combustion ammonia leads to remarkably higher temperatures if the same turbine inlet temperature is needed compared to other fuels, however, at the cost of significant NO_X formation, which may go beyond 100 ppm with thermal NO formation on par of fuel NO.

1. Introduction

One of the challenges associated with addressing climate emergencies is to find sustainable low-carbon energy sources that can supersede conventional fossil-based hydrocarbon resources. The combustion of renewable fuels has been recognised as a viable option to deliver a resilient energy source to the end-users, whether in a power plant or a simple boiler in households [1]. The progress and novel designs in renewable combustion can revitalise industries, utilities, and power plants to deliver green sustainable energy, which can be dubbed the green industrial revolution. Many potential fuels such as hydrogen, ammonia, bioethanol, and biodiesel are among the best nominations to replace the conventional fossil-based hydrocarbon fuels within the context of green growth [2].

Ammonia, produced from low-carbon sources, has been recognised as one of the promising replacements for fossil-based fuels since it carries no carbon molecule [3]. Ammonia energy content is comparable to gasoline and diesel fuels, making them a potential fuel where these hydrocarbon products are being utilised [4]. The exhaust gas from ammonia combustion is typically composed of nitrogen and water, as well as NO_X which needs to be kept in a controlled range [5]. The combustion of ammonia dates back to as early as 1941 when Macq [6] developed a catalytic convertor to crack the ammonia to hydrogen to assist the combustion process. In the following years, there has been a tremendous effort to analyse the fuel behaviour of ammonia, mainly in mobile combustion system applications, either as pure or blended with other fuels. It is reported that ammonia has a high octane number (>130) [7], thereby performing well under compression-ignition engines [8]. However, ammonia is associated with some drawbacks that may potentially limit its deployment in combustion systems for domestic applications, including low laminar flame speed [9], high ignition energy [10], and lower combustion temperature [11].

Several studies explored limiting NO_2 formation during ammonia combustion, by either re-burning or quenching NO_X [12]. It has been suggested that reducing nozzle diameter and increasing nozzle distances between fuel and air injectors can reduce NO_X formation [13]. Choe et al. [14] showed that plasma application for ammonia combustion lowers NO_X formation and extends the lean blow-off limit. Mendiara and Glaborg [15] demonstrated that the choice of the oxidiser is influencing the NO formation in ammonia combustion. Ilbas et al. [16] found that

* Corresponding author.
** Corresponding author.
E-mail addresses: B.bazooyar@cranfield.ac.uk (B. Bazooyar), s.nabavi@cranfield.ac.uk (S.A. Nabavi).

https://doi.org/10.1016/j.joei.2022.10.008
Received 30 April 2022; Received in revised form 14 October 2022; Accepted 18 October 2022
Available online 22 October 2022

ammonia addition to kerosene in oxy and fired gas turbine combustor can change the NO_X concentration inside the flame zone and the flame position. However, they demonstrated that the NO_X at the combustor outlet is not much influenced by ammonia fraction in the fuel. Hussein et al. [17] have evaluated the mixture of hydrogen and ammonia combustion under the turbine conditions and reported that the minimum NO was observed at 60%–40% NH_3–H_2 and equivalence ratio 4%.

Ammonia premix flame can be stabilised in lean swirl premix pilot burners [18]. Valera-Medina et al. [19] have demonstrated using OH* Chemiluminescence that the stability region of ammonia flames is quite narrow and it can be achieved using strong swirling flows. Tang et al. [20] showed that arc gliding AC power is a useful technique to increase the stability region of ammonia/air flame and to extend its lean blow-off limit. Rocha et al. [21] verified three scenarios for ammonia combustion, namely dry low emissions (DLE); rich burn, quick quench, and lean burn (RQL); and moderate or intense low oxygen dilution (MILD) under the turbine conditions (inlet temperature 500 K and 20 bar). They revealed that the MILD and RQL combustion are good potentials for ammonia combustion in turbine conditions as they limit the thermal NO formation. Regarding nonpremix combustion, the data associated with ammonia combustion is rather limited. Ilbas et al. [22] numerically modelled the combustion of ammonia oxy-flame with pure oxygen and air-flame. They highlighted that flame stabilisation and NO_X emissions are two potential problems that are needed to be addressed for the successful delivery of ammonia in nonpremixed systems. Chen et al. [23] suggested that NO_X emissions can be reduced when enhancing NH_3 combustion efficiency.

There is not much information about the flame characteristics of ammonia in boilers and small scale micro gas turbines. This work aims to determine the combustion behaviour of ammonia under boiler and turbine conditions and provide in-depth insights into whether ammonia can be a long-term solution for ever-increasing energy. A 50 kWth boiler and 12We microturbine combustor were chosen to conduct the case study and analyse ammonia flame characteristics. First, the ammonia mixture temperature, laminar flame speeds, and ignition delay time for these two units have been obtained and compared with hydrogen, biogas, methane, syngas and dimethyl ether. Furthermore, the combustion flame analysis was performed for the boiler and turbine, in terms of flame stability analysis, and ignition modes.

2. Analysis procedure

This study was to reveal the characteristics of ammonia combustion by divulging the flame features in boilers and turbines and comparing and contrasting ammonia and other prevalent fuels for domestic applications. The boiler was designed to burn diesel, kerosene, and natural gas when the suitable burner is used. The microgas turbine was designed to release the energy of the biogas and to power a 12 kWe expander shaft. The modelling of the study has two parts. First, the potential of ammonia as a renewable fuel will be analysed using several ideal reactors. This translates the combustion to a simple mixing problem, making it easier to compare and comment on the flame characteristics. Afterward, the ammonia combustion was numerically modelled in real turbine and boiler applications.

The operating pressure of the boiler and microgas turbine were 1 and 3 bar respectively. Fuel and mass flow rates, oxidiser, and fuel temperatures were set according to the operating units of the combustion system. The temperature for air and fuel in the boiler was considered 283 K. For the turbine, the fuel and air temperatures were 283K and 920 K (considering pre-heated air).

2.1. Reactor modelling

The ammonia combustion was modelled using an equilibrium reactor to compare the adiabatic flame temperature with that of other gaseous fuels. Afterward, a closed partially stirred reactor (PaSR) was used to analyse the ignition delay time or the timescale takes that ammonia ignites when mixed with different air ratios. Finally, a sample premix laminar-burner stabilised flame was used to calculate the ammonia flame speed. All these characteristics were obtained over a range equivalence ratio typical for ignition initiation in gas turbines and boilers. If any, fluctuations were also captured by considering a wider range of air to fuel ratios and making the analysis cover any unforeseen oscillations in operating conditions. The chemistry of the combustion for the fuel flames will be given in the next section.

2.2. Numerical methods

2.2.1. Model setup

The computational fluid dynamics (CFD) modelling of a boiler and turbine were carried out using Reynold-Average-Navier-Stokes turbulence approach in conjunction with the Flamelet concept [24,25] to capture the precursor species. The k-ω Shear Stress Transport (SST) model [26] was used to exploit both the advantage of efficient wall function in k-ω model as well as the free-shear well predictability of k-ε model [27]. For analysis of the flame in terms of precursor species and mixing problem, detailed mechanisms for chemical reactions have been utilised. Table 1 tabulates the specification of mechanisms used to generate 10 nonadiabatic flamelets with 32 grid points. The compressibility effect was also considered to deliver the influence of pressure. For this study, the Peng-Robinson equation of state has been used for PDF-mixture density to show the influence of pressure increase under operation in gas turbine conditions. The models were previously validated in the gas turbine combustor against 32 operating points for the combustion of different mixtures of methane and carbon dioxide with different mass flow rates and oxidiser temperatures [28,29].

Four transport equations for NO, NH_3, HCN and N_2O were solved for prediction of NO_X for all fuels. The turbulence-chemistry interactions of these species were resolved using the Gaussian PDF density function. The transport equations give the evolution of species contributing to the formation of NO through thermal, prompt, and N_2O pathway mechanisms and include the advection terms, diffusion, and source terms for mass fraction of the species [34]. The time-averaged transport equation of NO is used to show the NO_X plume. Thermal NO and N_2O pathway mechanisms have been employed in the combustion of all fuels in simulations. The prompt NO was employed for methane, DME, and syngas. The extended Zeldovich mechanism [35] was used for thermal NO_X, and DeSoete [36] formulations were employed for prompt NO and N_2O pathway in reaction source term. For ammonia, the fuel NO_X formulations and thermal and N_2O pathway were considered. The discrete ordinates radiation model [37] was also used in the source term of the energy balance equation to enhance the predictability of NO_X emissions. A detailed description of governing equations and mathematical modelling can be found elsewhere [38]. A more comprehensive description for NO_X formation in boilers can also be found at [39–41].

2.2.2. Computational domain and boundary conditions

Fig. 1 presents the schematic of the boiler and microgas turbine combustion chamber used for combustion analysis. The boiler and

Table 1
The combustion mechanisms used to generate flamelets.

Fuel	Mechanism	Number of species	Number of reactions	Reference
Ammonia	Nakamura-2017	38	232	[30]
DME	Kaiser-2000	79	351	[31]
Methane	GRI MESH 3.0	53	325	[32]
Hydrogen	Kéromnès-2013	17	49	[33]
Syngas	Kéromnès-2013	17	49	[33]

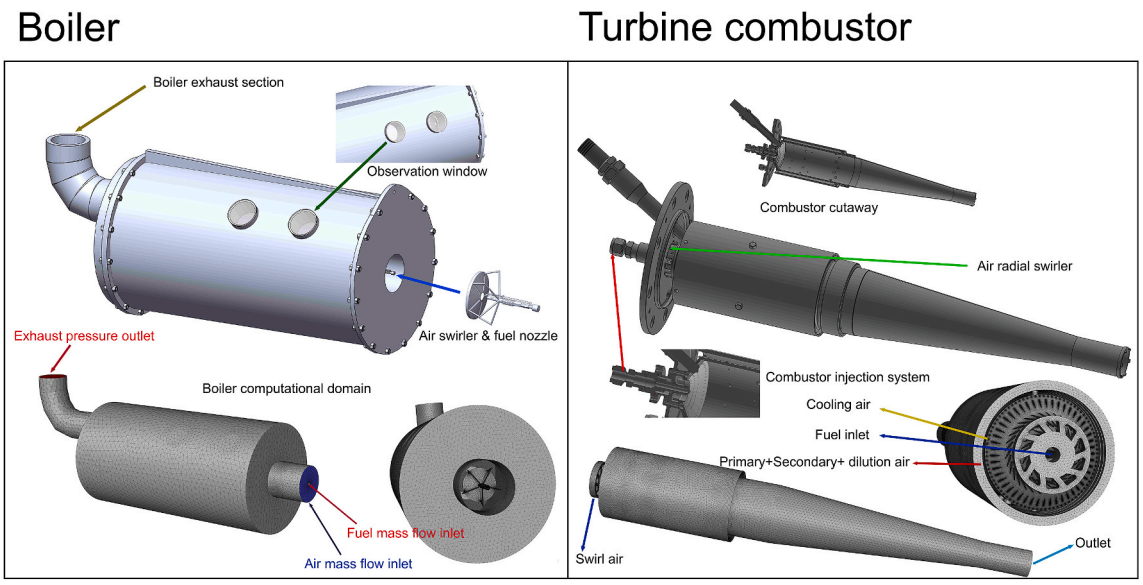

Fig. 1. Schematic of the boiler (left) and microgas turbine combustor (right).

turbine combustor geometries have been created using Solidworks. The ANSYS Fluent 2021 R2 was used for domain definition, mesh generation, model setup, solution, and post-processing.

The 45 kWth boiler includes a cylindrical combustion chamber with a pressure swirl burner. The burner is equipped with a coaxial swirler and hollow cone nozzle for spraying the fuel into the chamber. The angle between the swirler vanes and an artificial plane perpendicular to the air stream is 37.5°. The combustion chamber has two windows for the observation of the flame. The combustion began with an electric arc and was sustained via hot gas recirculation coming back from the chamber rear walls.

The 12 kWe gas turbine combustor includes the cylindrical liner surrounded by an annulus to stage the air at three series of holes to avoid stochiometric combustion-1. Primary holes, 2. Secondary holes, and 3-dilution holes. The liner conic head also includes 221 inclined holes to cool down the inner liner walls to promise a long-term operation of the gas turbine combustor under a harsh combustion environment (high pressure and temperatures). The ignition began with an electric arc, and sustainable combustion was achieved by injecting recuperated heat from the swirler and other combustor holes.

2.2.3. Solution algorithm and monitoring

The second-order upwind is employed to discretise the space derivatives of advection terms in the transport equations. A double-precision steady-state solver with a coupled algorithm in an iterative algorithm is utilised to solve the equations. The PRESTO (PREssure Staggering Option) and PISO (Pressure Implicit with Split Operator) algorithms are employed for pressure and pressure–velocity coupling, respectively. The residuals for continuity, momentum, and transport of mixture fraction, mixture fraction of variance, and NO are set 10^{-3} to obtain convergence in the solution. For the energy equation, the residual for the solution was considered 10^{-6}. A monitor including the area-averaged temperature at the micro combustor outlet is defined to assure the completion of the simulation. The simulation is initiated by the temperature patch of 2000 K at the entire domain. The simulations are considered complete at each operating point when the area-averaged-total-temperature at the outlet was constant, and the residuals of the differential equations met the pre-defined conditions.

2.2.4. Mesh sensitivity analysis

The simulation has been performed in grids containing hexahedral elements for both boiler and turbine combustors. The values of pressure, temperature and concentration of NO were compared for a different number of elements. For the boiler, the grid containing ~660,000 to 5,000,000 elements was considered. For microgas turbine, the grid, including 1,200,000 million to 11,000,000 elements, was used for verification. The preliminary analysis has authenticated that over 1,000,000 elements in the boiler geometry and 5,000,000 million in the turbine combustor geometry result in less than 5% difference in the variables. Therefore, the boiler grid with 2,000,000 elements, and microgas combustor with 6,000,000 elements were used for numerical modelling. The computational costs were 5 and 8 processor hours for boiler and gas turbine combustor with Intel(R) Core(TM) i9-7980XE CPU @ 2.60 GHz, 24.75 MB cache.

3. Results and discussion

3.1. Air and fuel mixture adiabatic temperature

Fig. 2 presents the adiabatic flame temperature or mixture temperature. The trendline associated with the equivalence ratio for the fuels is demonstrated in boiler and turbine conditions. Indeed, ammonia gives the least flame temperature compared to the other fuels. The stochiometric flame temperature for ammonia, methane, DME, syngas and hydrogen were 2067, 2212, 2283, 2304 and 2360 K under boiler conditions. The stochiometric mixture temperature for ammonia, methane, DME, hydrogen and syngas 2076, 2233, 2403, 2390 and 2340 K, respectively, under turbine conditions.

The deviation among the flame temperature for the fuels in higher equivalence ratios is emboldened, which begins from the stoichiometric ratio (ER = 1). When the flame is saturated with the fuel, a close mixing temperature for the fuels was expected. The influence of the pressure on the flame temperature is somehow evident in increasing both the flame temperature, and the difference that exists among the fuels. The increase rate for the fuel with higher flame temperatures is slightly higher than those with lower flame temperatures.

3.2. Flue gas composition

The flue gas composition from the combustion of fuels is a determining factor in the operation of both turbines and boilers. Under boiler conditions, the fuel gas radiative potential is influenced by its composition and might change the rate of the steam. In turbine conditions, on the other hand, this may lead to different heat transfer properties and

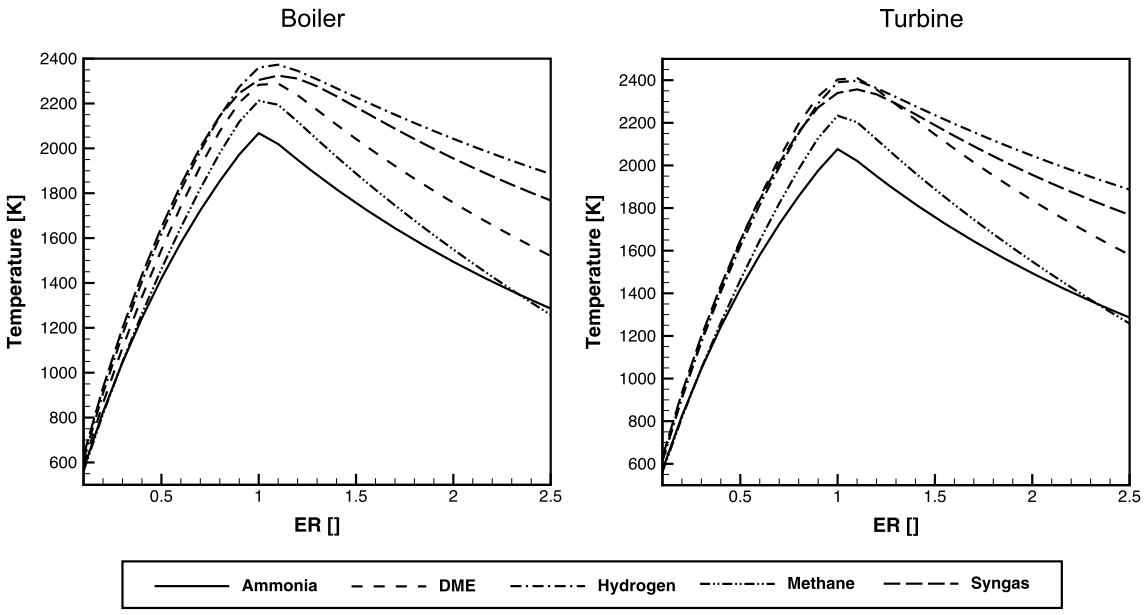

Fig. 2. The adiabatic flame temperature of ammonia, DME, hydrogen, methane and syngas at equivalence ratios [0.1 2.5].

concomitant blade cooling design points. Similarly, the flue gas composition can determine the heat recuperation potential from the exhaust of both boiler and turbines. Fig. 3 gives the trendline of the flue gas composition of ammonia in comparison with other fuels. As expected, nitrogen is the dominant flue gas species for all fuels when combustion is fuel and air rich. The ammonia flue gas is generally similar to that of hydrogen, having the same N_2, water, and O_2. However, it is different from syngas, methane, and DME in the presence of carbon dioxide. Indeed, the water in the flue gas with higher heat capacities can conserve the heat for recuperation while it may lead to lower spatial temperatures and the potential of combustion for heating purposes. In the microgas turbine, this is an adventitious feature of ammonia as it may lead to a lower turbine inlet temperature.

3.3. Autoignition delay

Autoignition is the main flame stabilisation mechanism in the majority of burners [42]. The ignition delay time is an important combustion parameter that can determine the behaviour of different fuels, particularly in gas turbines. A short ignition delay time may lead to fuel autoignition in the premixer of gas turbine combustors, damaging the hardware and turbomachinery. This section explores how ammonia behaves if it is mixed with air before combustion. This may not influence the combustion under the selected boiler as it works in nonpremix mode. However, it should not be significantly long to avoid flame lift and blow off. The ignition delay time as a function of the equivalence ratio is provided in Fig. 4. The ignition delay time of ammonia is comparable to that of methane, and it is longer than hydrogen, syngas, and DME. The same order of magnitude in the ignition delay time of ammonia and methane under turbine conditions indicates that ammonia can be utilised in existing gas turbine combustion units that are designed for methane. Reiter et al. [43] have also shown that the ignition of ammonia in diesel engines is not as easy as in conventional hydrocarbon fuels. Further, they highlighted that to prevent the engine from misfiring, adequate ignition energy should be provided to the ammonia-air mixture cylinder.

Wobbe index is another fuel characteristic that needs to be kept in the same range when superseding any potential fuels to the existing ones in the gas turbine combustors, Table 2. This shows the pre-combustion features of the fuel and their suitability in the gas turbine combustors. According to Table 2, Wobbe index of ammonia is much lower than that of methane and hydrogen. Hence, the application of NH_3 in gas turbine combustors is expected to be challenging. This issue can be addressed by stimulating the combustion of ammonia in a real gas turbine and revealing its characteristics.

3.4. Laminar flame speed

Laminar flame speed is a combustion parameter that determines the flame propagation area and mechanisms. Most of the flames are turbulent and determining the real flame speed is highly practical that depends not only on the fuel but also on the combustion characteristics including pressure, temperature, and combustor. Here, laminar flame speed is used to comment on the stability range of the fuels for the combustion system. Fig. 5 gives the trendline of laminar flame speed for ammonia, DME, hydrogen, methane, and syngas. The stability region of

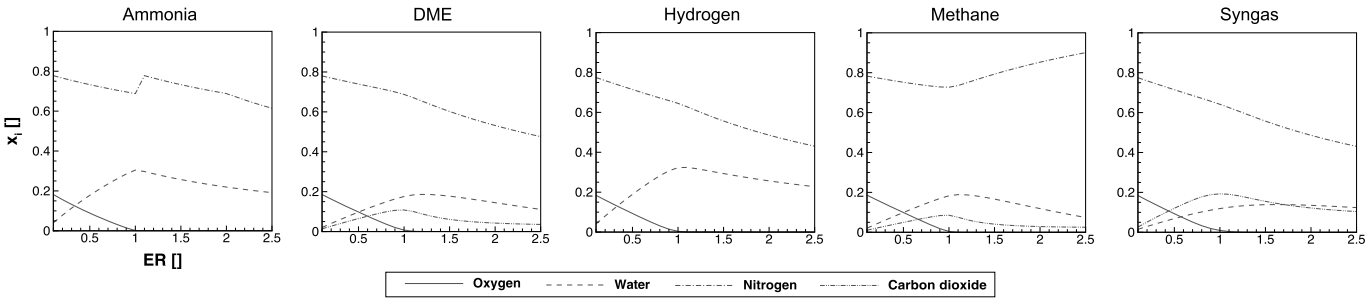

Fig. 3. Flue gas composition of ammonia, DME, hydrogen, methane and syngas over equivalence ratios [0.1 2.5]. x represents the spatial mole fraction of the specie i.

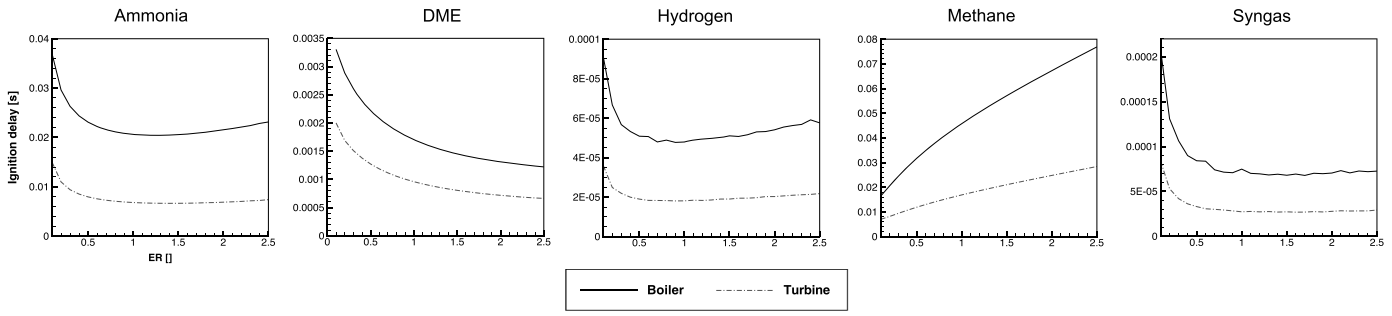

Fig. 4. The ignition delay time of ammonia, DME, hydrogen, methane and syngas over equivalence ratios [0.1 2.5].

Table 2
Calculated Wobbe indices of gaseous fuels were used in this study. Wobbe index is the ratio of the higher heating value to root square of the specific gravity.

Fuel	Ammonia	DME	Hydrogen	Methane	Syngas
Wobbe index	19.99	14.53	43.88	49.10	11.13

ammonia as a fuel as well as its flame speed is a bit lower than that for methane and much lower than hydrogen. This may make the ammonia behave such as heavy fuels that necessitates some modification to the fuel injection systems and air blowing mechanism. The laminar burning velocity of ammonia was 20 and 17 cm/s under boiler and turbine combustion conditions, respectively. Li et al. [44] stated that the low burning velocity and flame temperature of ammonia limits its application in energy device. They also proposed that the increasing the oxygen content of the oxidizer can compensate the negative effects ammonia due to its thermophysical characteristics.

3.5. Ammonia in the boiler

The combustion of ammonia in the boiler is analysed in terms of temperature, burning velocity and NO_X emissions, Fig. 6 7 and 8. The combustion mode was also analysed to find the main burning mechanisms of ammonia compared with other fuels. Fig. 6 gives the temperature contours for ammonia combustion in the boiler. The temperature at two perpendicular planes YZ, XZ and ten transverse planes, are given. The maximum temperature was around 2000 K which is slightly lower than that for the combustion of other fuels (ammonia, DME, hydrogen and methane). The maximum temperature for ammonia as well as for other fuel corresponds to the centre of the chamber where the swirl air surrounds the fuel turbulent jet. The fresh flow of the oxidiser will mix with recirculated gas coming back from the combustion chamber rear wall and finally react with the fuel jet. This leads to the flame stabilisation in the boiler. In case of the boiler combustion chamber, the oxidiser momentum is high enough to limit radial diffusion of the fuel towards the side walls. This results in the rather higher intensity of the combustion and higher spatial temperature at the centre of the chamber. This is in agreement with experimental evaluations with this boiler for biodiesel fuel and blends of biodiesel with diesel [45–49]. The boiler temperature at transverse planes with a distance of 10 cm is also given. The length and width of the ammonia flame are comparable to that of methane, although its local temperature is slightly lower, Fig. 8.

The velocity contours, vectors and streamlines during ammonia combustion are shown in Fig. 7. The streamlines exhibit the central jet is branched well before the combustion chamber rear walls with one branch goes to the exhaust section and other to come back forming a recirculation zone. The recirculated material from ammonia combustion reacts with the fresh reactant coming from the gas burner resulting in the flame stabilisation. The contour plots of the velocity magnitude shows that the central jet has comparatively higher momentum than the recirculated materials. Thus, the diffusion of reacted materials into the central is main flame stabilisation mechanism. This gives rise to a high flame length in the boiler and elongated reactive zone which is proper for radiation and heat transfer. The streamline in the transverse planes also confirms the swirl air can well cover the central fuel jet stream and widen the flame with enough degree of luminosity. The swirl flow of the air can sustain towards 70 cm far from the chamber front wall. This is while the flame length rarely passes 60 cm.

The NO_X emissions contours are given in Fig. 8. The NO_X emissions for ammonia involve fuel NO_X, thermal and N_2O pathway mechanisms. The contours show that the level of NO_X could be around 0.2% of the flue gas in the vicinity of the air swirler. However, the level is going down significantly in the boiler exhaust section to around 100 PPM. In this case, the fuel NO_X is the dominant formation mechanism in the flame area, indicating that the nitrogen atom dissociation from the ammonia resulted in significant NO_X formation at the flame boundaries. However, in the exhaust section and post flame zone, a part of NO_X was re-burnt and turned into nitrogen molecules. Ilbas et al. [22] revealed that the area belonging to the stochiometric region is associated with significant fuel NO_X formation. In this region, it is expected that the level of thermal NO_X to be lower than the fuel NO_X. Moreover, Chen et al. [23] highlighted that the significant NO_X emission of pure ammonia in nonpremix combustion is proportional to the degree of completion of the combustion.

To have a better understanding of ammonia combustion compared to other fuels in the boiler, the temperature and NO_X emissions profiles

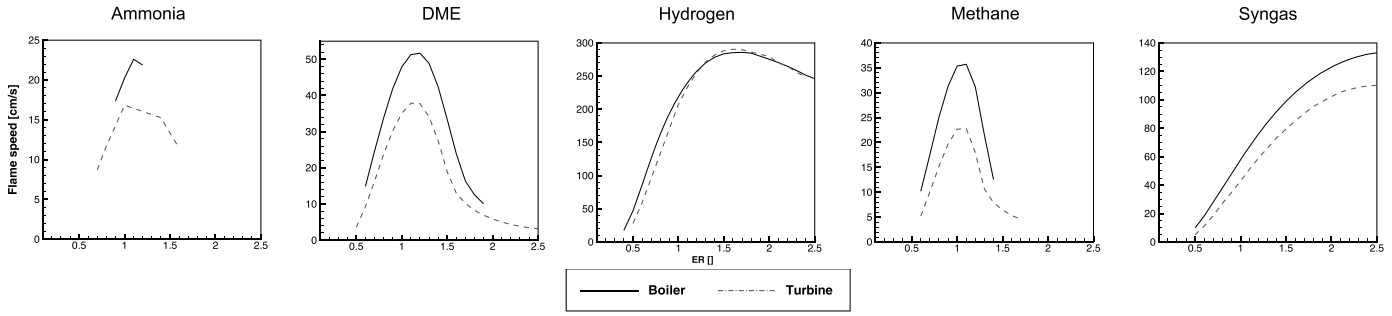

Fig. 5. The laminar flame speed of ammonia, DME, hydrogen, methane and syngas over equivalence ratios [0.1 2.5].

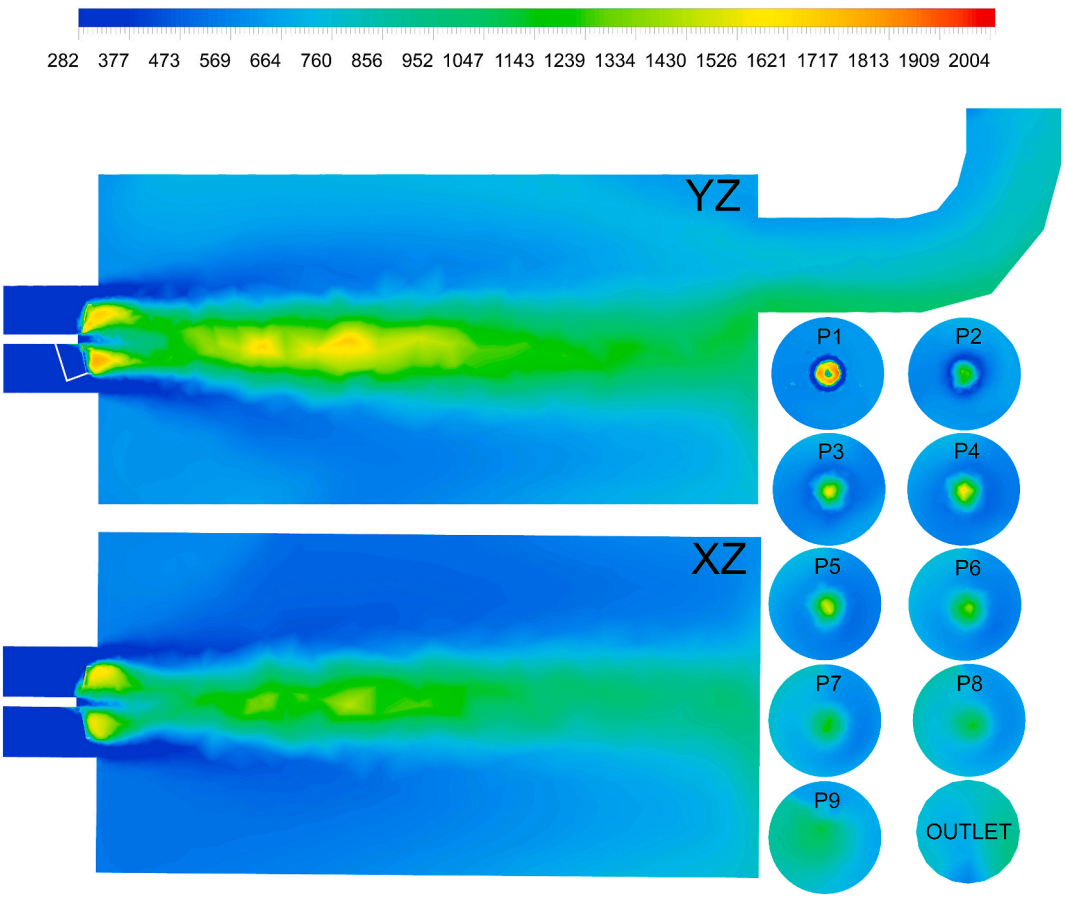

Fig. 6. Temperature contour [K] of the ammonia combustion in the boiler at YZ and XZ Planes, and 9 planes perpendicular to the air and fuel flow with a distance increment of 10 cm from the outlet plane.

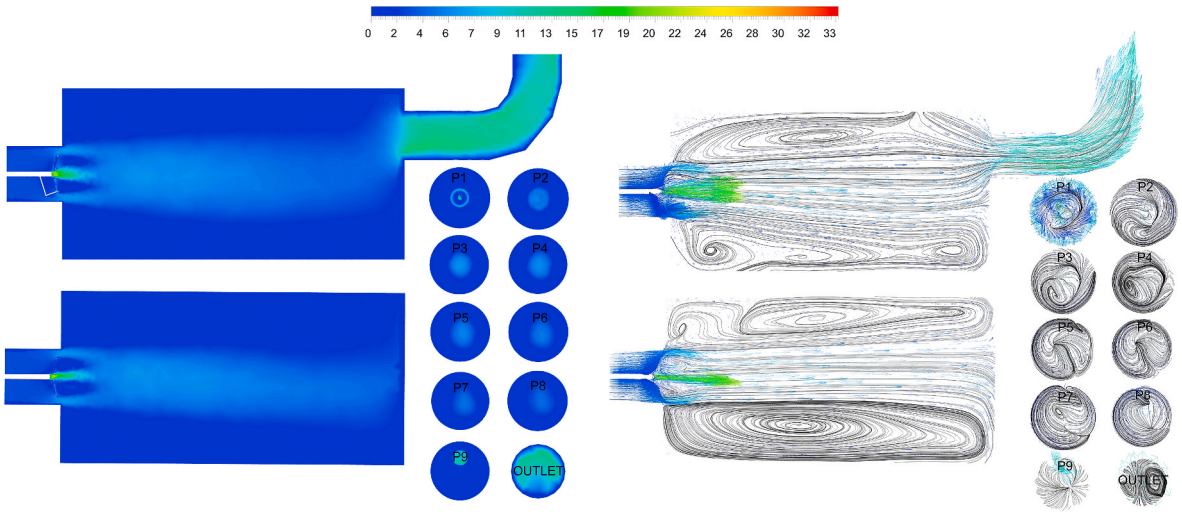

Fig. 7. Velocity magnitude contour, vector and streamline [m/s] of the ammonia combustion in the boiler at YZ and XZ Planes, and 9 planes perpendicular to the air and fuel flow with a distance increment of 10 cm from the outlet plane.

along the boiler are shown in Fig. 9. The values are obtained by averaging the temperature and NO_X emissions at 9 transverse planes, as presented in Figs. 7 and 8. The operation of the boiler with ammonia is similar to that of syngas in terms of both temperature and NO_X emissions. It should be highlighted that the fuel flow rates were identical for all the fuels. That's why hydrogen is associated with higher NO_X emissions and temperature compared to other fuels. The results also attest to ammonia's higher NO_X emissions compared with prevalent hydrocarbon counterparts, such as methane and syngas. This is mainly due to the fuel NO_X that may be controlled when a flame fuel-rich region can receive the produced NO_X.

The combustion mode of ammonia was also obtained using the normalised [-1 1] dot product of the fuel and air mass fraction scalar. The premix and nonpremix zone of the combustion was obtained using

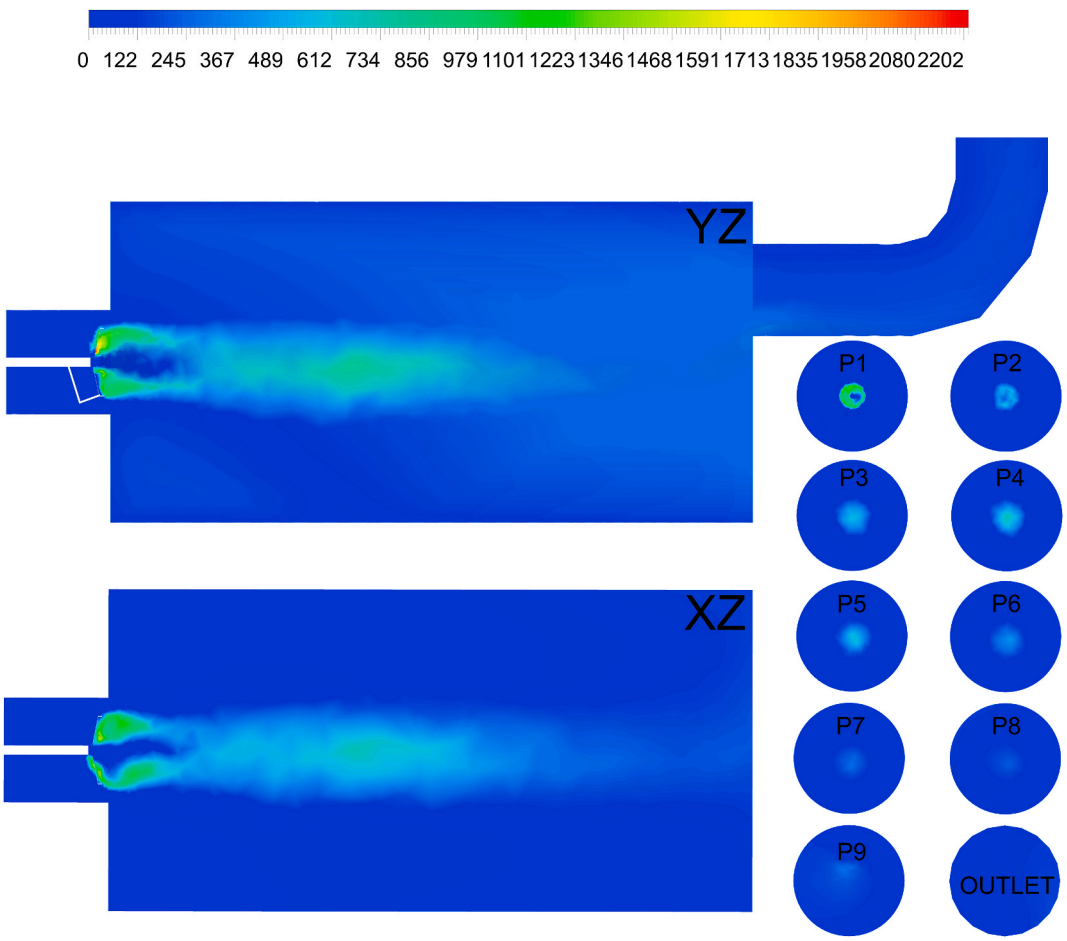

Fig. 8. NO_X emission [ppm] of the ammonia combustion in the boiler at YZ and XZ Planes, and 9 planes perpendicular to the air and fuel flow with a distance increment of 10 cm from the outlet plane.

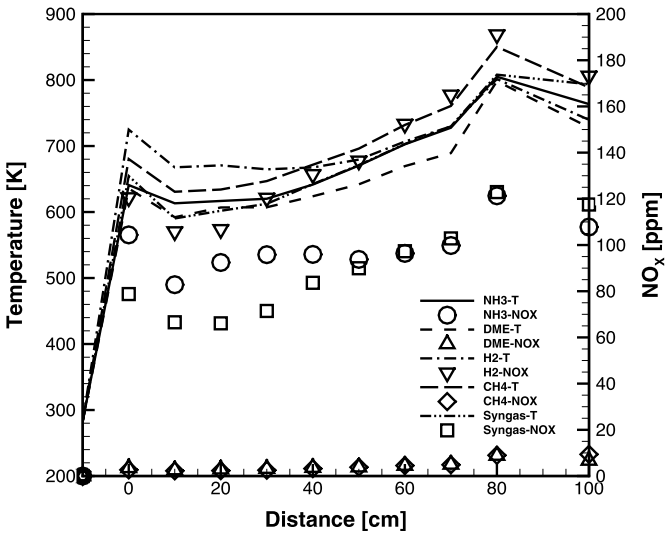

Fig. 9. The temperature and NO_X emissions averaged on the perpendicular planes along with the flow in the boiler for ammonia, DME, hydrogen, methane and syngas.

the positive and negative values of the flame index, Fig. 10. The primary combustion mode was expected by the nonpremix zone, which covers a slightly smaller internal zone. In the middle part of the flame cortex, where the mixing rate is high, the premixing zone is in the ascendency, whereas in the boundary between the air and fuel jet, the nonpremix zone appears. Fig. 10 also shows the oxygen mass fraction at the isosurface nonpremix zone and temperature at the isosurface premix zone. The premix zone contour, coloured by temperature, indicates that the flame in the premix zone is colder than the stoichiometric mixture of ammonia and air. In the premix zone, partial combustion takes place with spatial temperatures lower than the stochiometric mixture temperature. In return, the nonpremix zone boundary zone has the highest level of oxygen and fuel. The spatial temperatures at this region are high and near adiabatic flame temperature.

3.6. Ammonia in the turbine

In this section, ammonia combustion characteristics in a microturbine chamber for domestic application were explored and compared with other fuels. The fuel flow rate was set to achieve a turbine inlet temperature of ~1200 K for all the fuels. Accordingly, the mass flow rates were 3.70 g/s for ammonia, 0.53 g/s for hydrogen, 1.60 g/s for DME, 1.30 g/s for methane, and 6.00 g/s for syngas. The temperature at two perpendicular planes of YZ and XZ, and 9 transverse planes with a distance increment of 2 cm from the outlet is given in Fig. 11. For the turbine, the combustion was stabilised by the injection of recuperated air at 900 K. It was found that ammonia combustion temperature can reach as high as 2400 K. The region associated with the highest spatial temperature is observed between the primary and secondary holes, as it was observed for methane fuel. This is where the partial mixture of fuels with air can receive sufficient air for nearly complete combustion after which injection of additional air to the combustion environment can

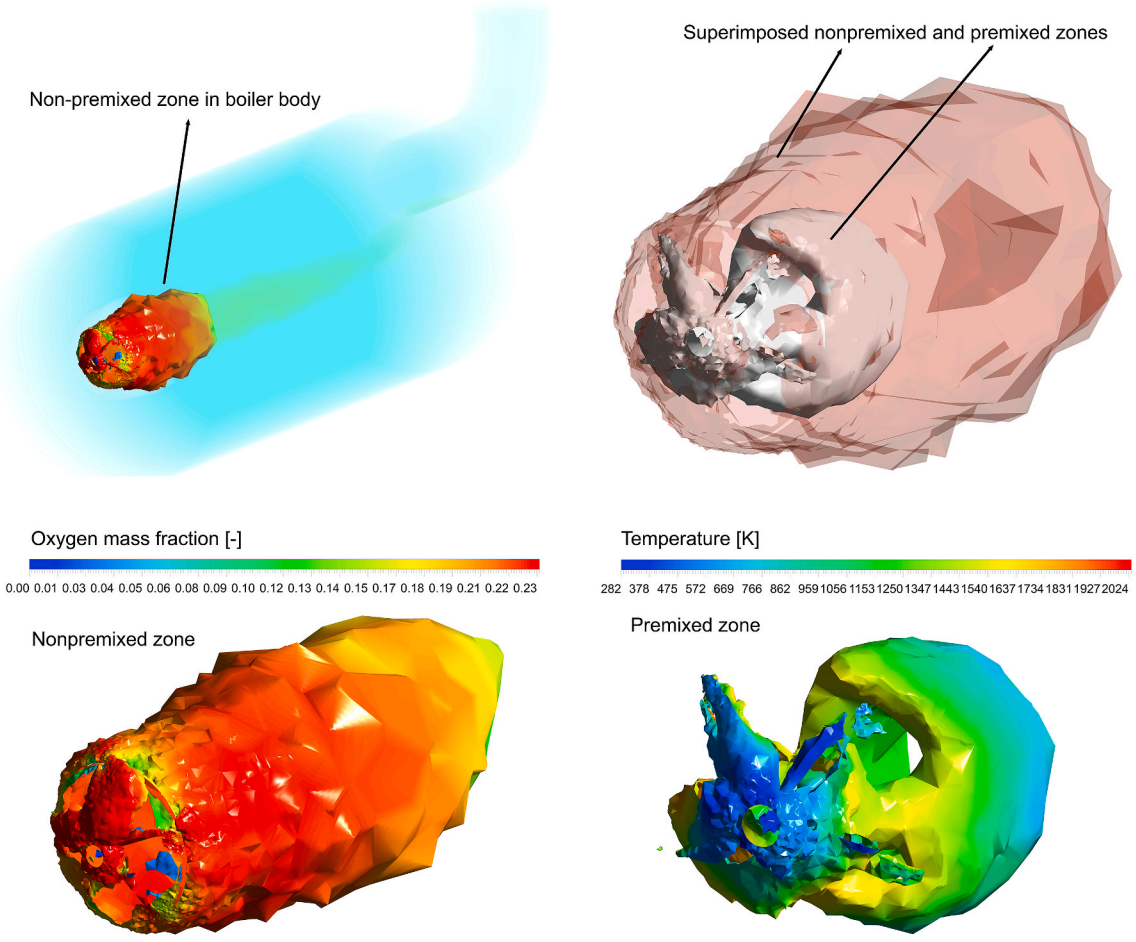

Fig. 10. Nonpremix and premix zones isosurfaces coloured by oxygen concentration and temperature.

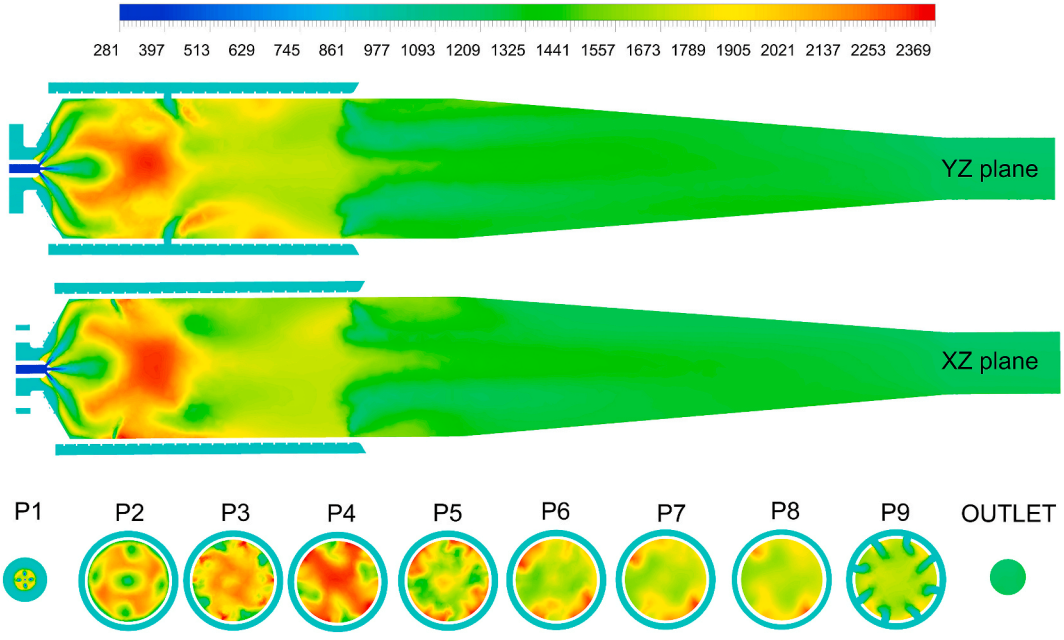

Fig. 11. Temperature contour [K] of the ammonia combustion in the turbine at YZ and XZ Planes, and 9 planes perpendicular to the air and fuel flow with a distance increment of 2 cm from the outlet plane.

cool the combustion mixture, reburn the NO_X, and set a proper turbine inlet temperature. This trendline confirms that ammonia can be utilised in the existing methane gas turbine burner.

Fig. 12 exhibits the contour, vector and streamline plots of the burning ammonia inside the microturbine combustor. There are two recirculation zones appeared in the liner which are different in radius, location, and direction. The larger one appears well behind the air jet which comes from the primary ports. It has a clockwise spanning which mix the inclined fuel stream well with the primary jet. The smaller one appears in the vicinity of the central axis. The anticlockwise spanning well mixes the central fuel jet with the circulated materials via the larger recirculation zone. The interaction of circulation zones makes the central and sidereal fuel jets contributing into the combustion chemical reactions and appearance of the flame over the entire width of combustion chamber. The streamlines in the combustor transverse planes also demonstrate that the penetration depth of the air jets from both primary, secondary and dilution hols is sufficient enough to diffuse into the central jet.

Fig. 13 shows the NO_X emissions contours plots of ammonia combustion in the microgas turbine combustor. It can be seen that the combustion in this burner can, to some extent, avoid the stochiometric mixing, and the presence of the dilution holes can re-burn the NO_X and drop its level. However, the NO_X emissions level is beyond the maximum limit of 100 ppm. The main reason for excessive emission is fuel NO_X formation, as also seen in the boiler case study.

The temperature and NO_X level for different fuels are compared in Fig. 14. It was found that ammonia is among the fuels with the highest temperature and nitrogen oxide emissions, which is mainly attributed to higher mass flow rates, for achieving similar turbine inlet temperatures as ammonia has the lowest heating value among the fuel. The higher mass flow rate of ammonia in the primary and secondary zone leads to intense combustion at a higher spatial temperature. This is also valid for NO_X emissions, as the higher temperature leads to a higher possibility of NO_X formation. The same observation was also valid for DME. This indicates that utilising the existing microgas turbine for ammonia and DME is not feasible to target NO_X emissions below 100 ppm. Okafer et al. [50] reported that ammonia in the gas turbine combustor is strongly influenced by the equivalence ratio instead of pressure, injection angle, and inlet temperature, therefore, NO_X formation may be controlled by optimising these parameters.

The combustion mode for ammonia is shown in Fig. 15. The nonpremix and premix zones are obtained from the flame index in the combustor environment. It was revealed that the primary ammonia combustion mechanism is premix flame propagation. Indeed, the dominant combustion mechanism in the gas turbine combustor is partially premixed combustion. The area associated with nonpremix combustion is relatively small, and partly located near the fuel nozzle and flame holder walls where the fluid is stagnant. This observation indicates that the existing microgas combustor can be used with ammonia, as an alternative to those conventional hydrocarbon fuels, in the same partial premix mode. However, a slight modification is needed to control NO_X levels and avoid high spatial temperatures.

3.7. Ammonia burning characteristics

One of the most important criteria for evaluation of turbulent combustion is the estimation and analysis of the turbulent flame speed. The uprising of the burning velocity as the fuel is injected into the combustor of both microturbine and boiler has been extracted from the numerical experiment and given in Fig. 16. The highest burning velocity in the Microturbine corresponds to hydrogen and lowest is for DME. The ammonia turbulent flame speed is comparable to syngas and methane in the turbine. Therefore, the flame propagation of ammonia is similar to methane. In the boiler, in contrast, the ammonia had the highest rate of burning velocity and propagation rate.

In terms of Mach number, the average values at the outlet plane of the microturbine combustor were employed to show the effect of fluid flow compressibility. The value for ammonia is similar to that for the syngas while DME had the lowest Mach number. The hydrogen fuel at the combustor outlet behaves as if methane was burned in the combustion chamber.

3.8. Ammonia NO_X emissions

To have a more comprehensive analysis of NO_X emissions of ammonia in investigated boiler and microgas turbine, volumetric mole fractions of NO obtained from fuel and dissociation of air nitrogen, i.e., thermal NO, are given in Fig. 17. The maximum level of thermal NO in the boiler and turbine was 7.5 and 170 ppm. The maximum fuel NO observed in the boiler and turbine was 240 and 280 ppm, respectively. The level of fuel NO is almost one order of magnitude larger than that of thermal NO. Moreover, the maximum NO is higher in the gas turbine combustor compared to the boiler. This is likely due to the ignition that is initiated with recuperated hot air in the gas turbine at 920 K compared to that in the boiler, begun with a cold swirling flow of air at 300 K. The other remarkable difference between the two combustion systems is that the level of deNO_X reactions or NO reburning is higher in the gas turbine combustor than the boiler. However, the outlet NO_X emissions in both cases are in the same order of magnitude-109 ppm and 77 ppm for boiler and turbine, respectively. The effective dilution in the gas turbine combustor also favours the destruction of a considerable amount of NO. Ilbas et al. [22] proposed oxy-ammonia combustion as an effective technique to target the required flame stabilisation and NO_X emission.

The mechanism of NO_X formation is different in the case of premixed

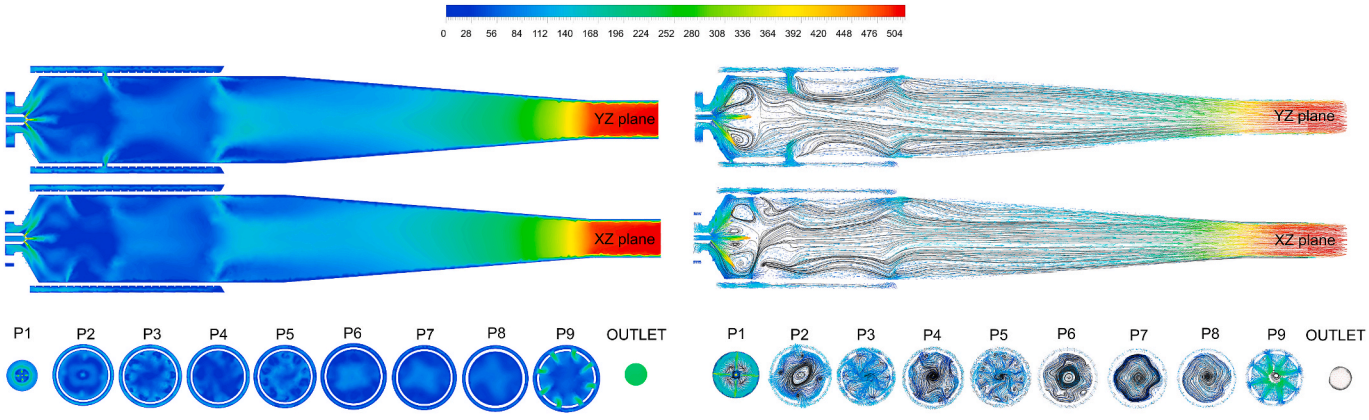

Fig. 12. Velocity magnitude contour, vector and streamline [m/s] of the ammonia combustion in the turbine at YZ and XZ Planes, and 9 planes perpendicular to the air and fuel flow with a distance increment of 2 cm from the outlet plane.

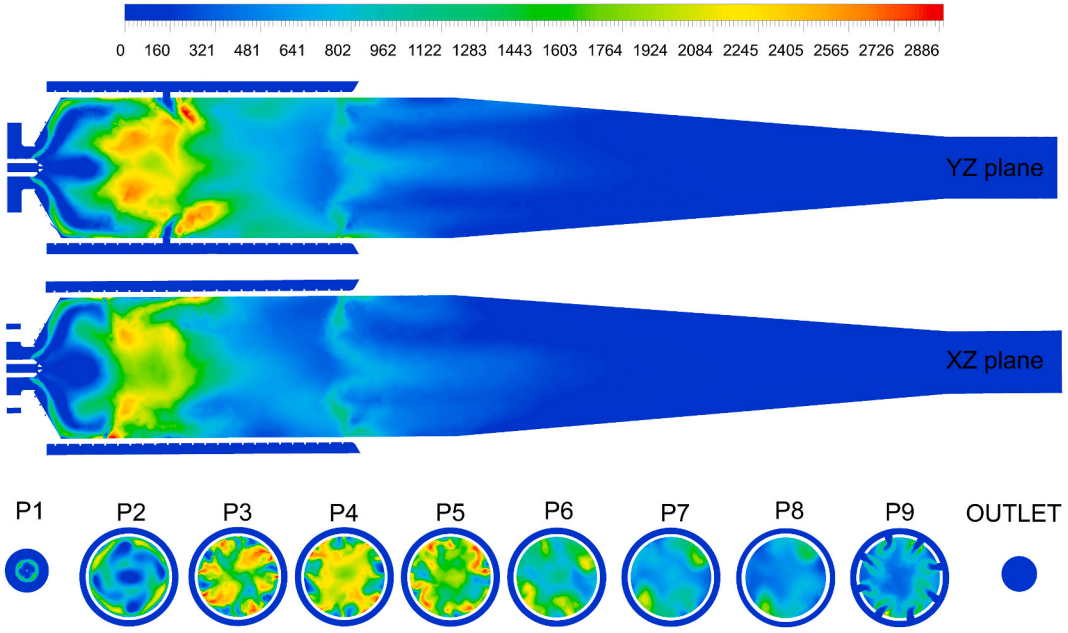

Fig. 13. NO_X emissions [ppm] of the ammonia combustion in the turbine at YZ and XZ Planes, and 9 planes perpendicular to the air and fuel flow with a distance increment of 2 cm from the outlet plane.

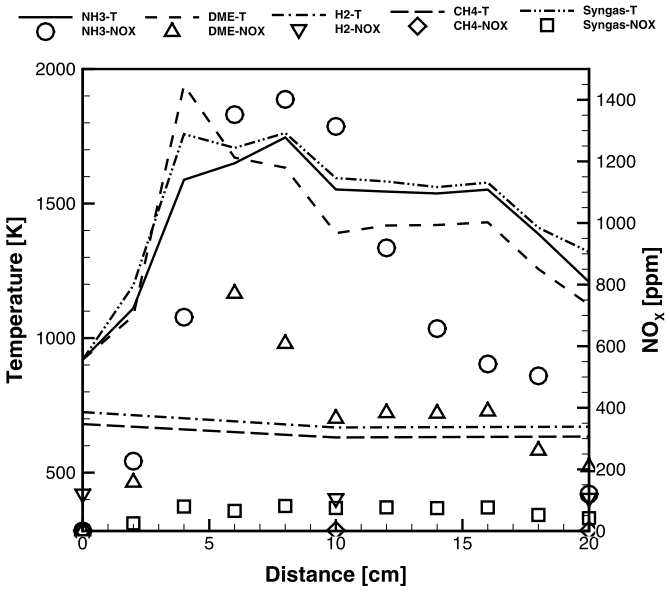

Fig. 14. The temperature and NO_X emissions, averaged on the perpendicular planes, along with the flow in the turbine for ammonia, DME, hydrogen, methane and syngas.

and nonpremixed combustion. In non-premixed combustion systems, local stratified regions are formed where ternary mixing between the ammonia, oxidiser, and recirculating materials occurs, resulting in NO_X reduction through reburning. In premix combustion, on the other hand, the localized combustion is namely a-priori which is governed by the combustion global equivalence ratio. In this case, the stratified zones, if ever forms, are extremely narrow which limits NO_X reburning. Similarly, Xiao et al. [18] confirmed that one effective technique to reduce NO_X emissions is to develop a new stratified injection technique for reburning of nitrogen oxides.

The NO formation for the studied boiler is largely within the flame stochiometric zone. At this region, it is expected that the combustion is under stochiometric. For the turbine combustor, the high NO area occurred near the liner walls, where the fluid is almost stagnant or an established recirculation zone. Bazooyar and Darabkhani [27] confirmed that near the primary and secondary ports of this combustor, a recirculation area was formed, likely due to the collusion of incoming gas to the vertical movement of the air through the ports. How this may lead to more spatial NO emissions in the chamber can be answered by the local residence time for the combusting mixture. In this region, the temperature is adequately high for the dissociation of nitrogen, and potentially chain branching reaction among atomic nitrogen and oxygen [52].

From the level of NO, which is the result of incomplete combustion of ammonia, it is expected that the combustion efficiency over the entire combustor is near 100%. The ammonia level at both combustor outlets is near zero, making the heat loss from the exhaust almost negligible. The preliminary calculation of combustion efficiency confirmed that when ammonia is entirely consumed in both boiler and turbine, the combustion efficiency reaches 100% and does not fall along with the flow. The combustion efficiency for ammonia combustion can be obtained from the following equation:

$$\eta = 1 - \frac{Q_{NO}[NO] + Q_{NH_3}[NH_3]}{Q_{NH_3}\left[\left(N_2 - [N_2]_{feedstock}\right) + NH_3 + NO\right]} \times 100\% \quad (1)$$

where $Q_{NH_3} = 382.6$ kJ/mol, $Q_{NO} = 57.09$ kJ/mol, [x] represents the spatial mole fraction of the specie x in the chamber, and $[N_2]_{feedstock}$ is the mole fraction of nitrogen in a mixture of fuel and oxidiser.

The comparative level of thermal to fuel NO in both the turbine and boiler at 10 transverse planes is presented in Fig. 18. In the boiler, the level of thermal NO is remarkably lower than the fuel NO. In contrast, in the gas turbine, the level of thermal NO is comparable to the fuel NO, with a ratio of ~0.2. As previously discussed, the spatial temperature associated with ammonia combustion is relatively high, which cause comparatively larger level of thermal NO compared to fuel NO.

Compared to the boiler, the ratio of the thermal/fuel NO in the gas turbine combustor is higher and observes a relatively higher fluctuation while the overall trend is increasing towards the discharge nozzle. This is higher as the occurrence of combustion in the gas turbine is with a very hot air at 920 K while the fuel in the boiler ignites with a cold stream of air with the aid of hot circulated materials at nearly 600 K. The

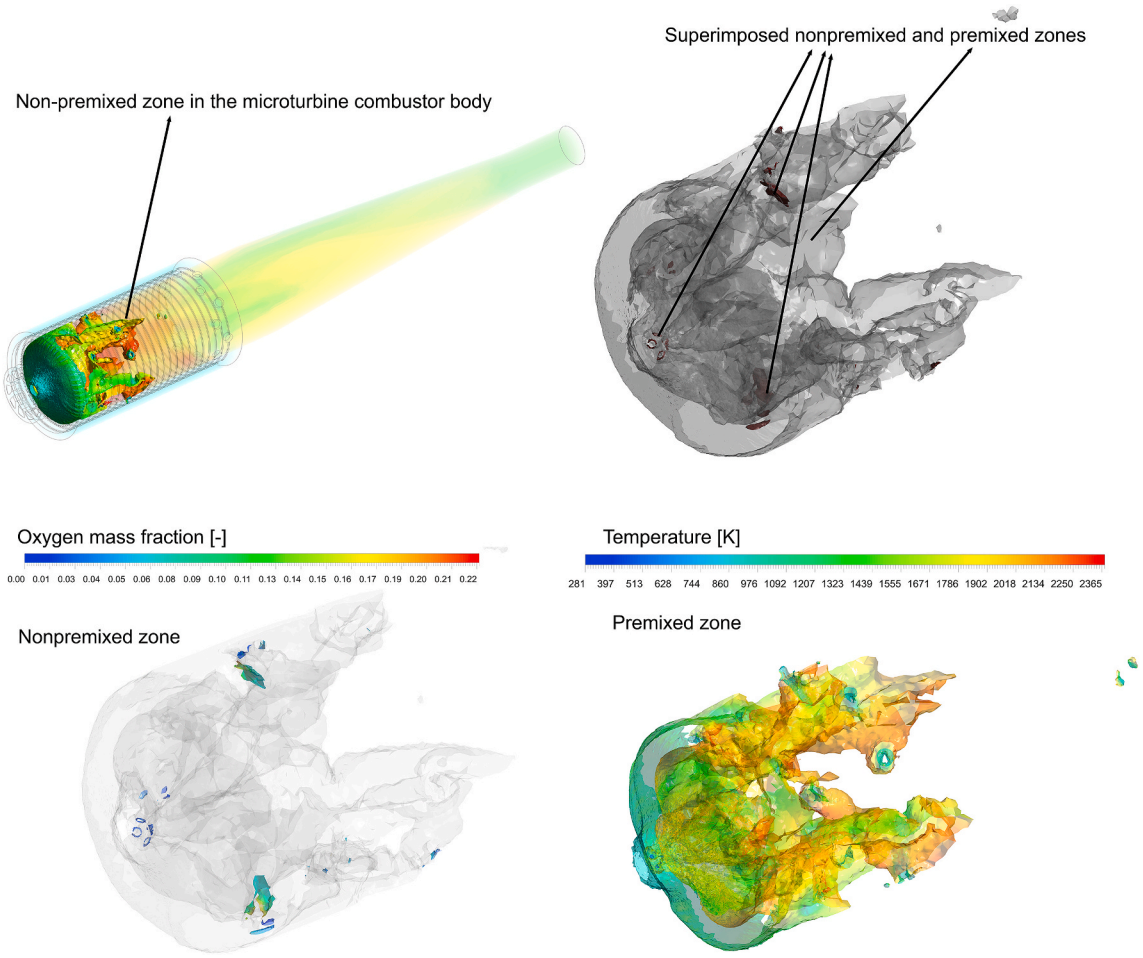

Fig. 15. Nonpremix and premix zones in the gas turbine combustor isosurfaces coloured by oxygen concentration and temperature.

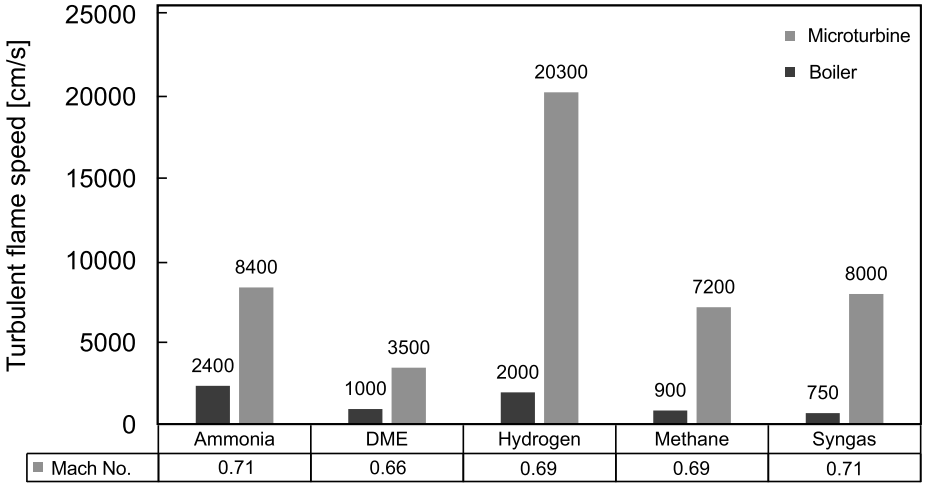

Fig. 16. Turbulent flame speed [cm/s] of ammonia compared to DME, Hydrogen, Methane and Syngas in boiler and microturbine combustor along with the outlet Mach number at the microturbine combustor outlet.

injection of hot air at the microturbine combustor has both decreasing and increasing effect on the NO_X emission. It has decreasing effect as it can suddenly cool the reactive mixture, while this increases the effect further downstream as the fresh stream of the air reacts with partially mixed fuel and air and complete the combustion towards the end.

Apart from the combustion characteristics and emission, what a new fuel necessitates in the operation of the entire combustion system is the synergy among the combustor and equipment installed to harness the power. This is indispensable, especially in the case of a gas turbines as any change in turbine inlet temperature and combustor mass flow rate might change the tubine/compressor fitting, blade cooling circuit, heat exchanger network, and operation of the entire turbomachinery [51]. Further work on ammonia combustion for the application on the gas turbines should provide technical information beyond the combustion to

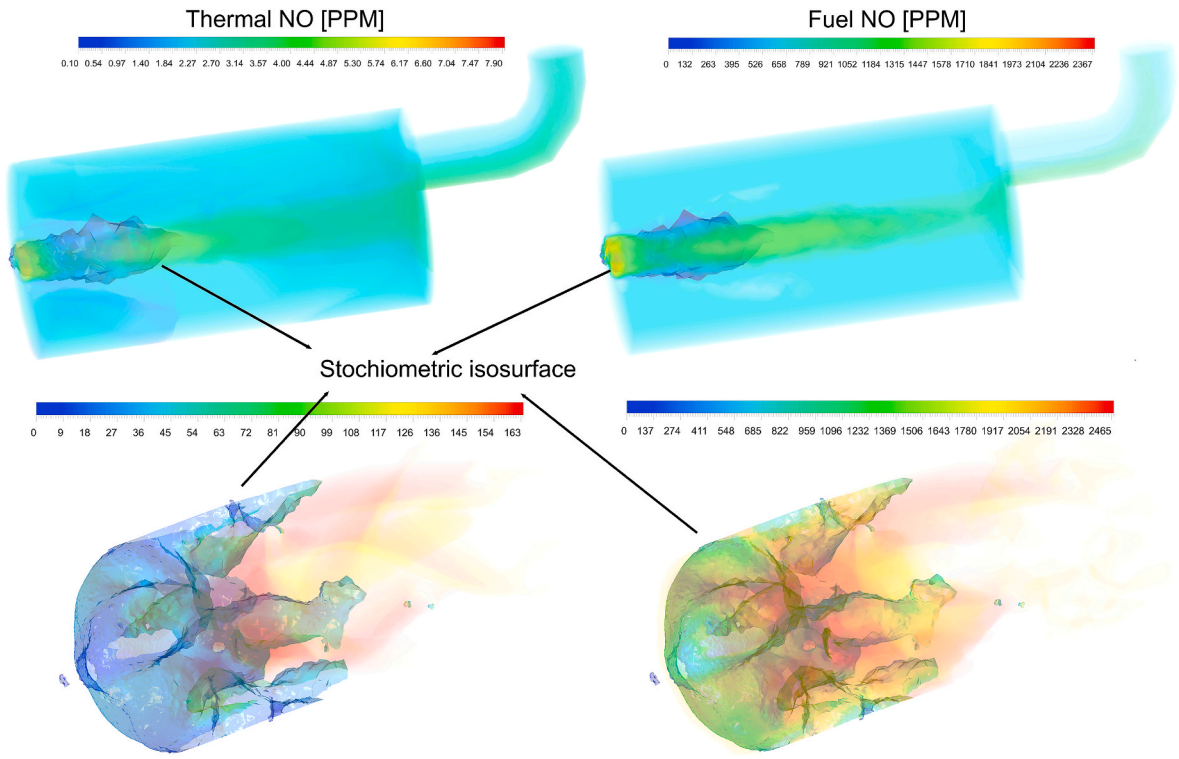

Fig. 17. Volumetric thermal and fuel NO mapped on the stochiometric isosurface with equivalence ratio = 1.

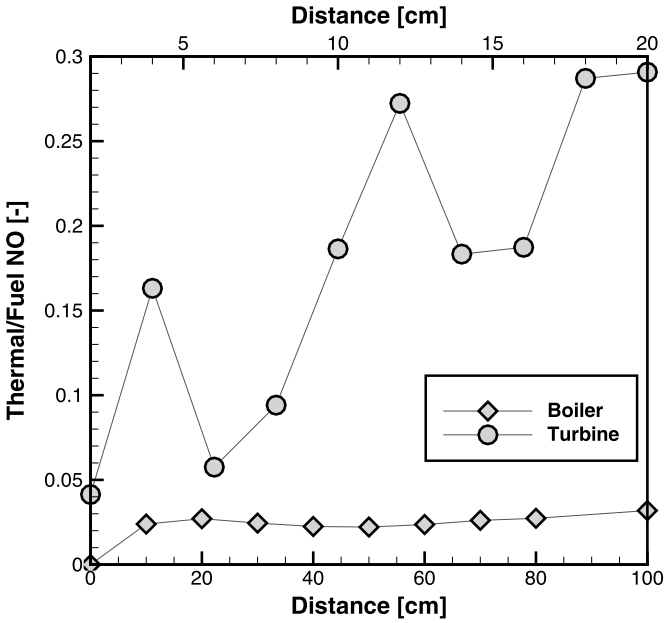

Fig. 18. The thermal and fuel NO ratio, obtained by averaging the thermal and fuel NO values at 10 transverse planes.

deploy this renewable fuel as an energy career to the grid.

4. Conclusions

This work provided a comparative analysis of ammonia combustion in microgas turbine combustors and boilers for domestic application. First, the ammonia combustion characteristics including the mixture temperature, laminar flame speed, autoignition delay were compared with DME, methane, hydrogen, and syngas. Then the performance of ammonia combustion in gas turbine and boiler were numerically compared with those fuels. The flue gas composition of ammonia and hydrogen is highly similar, containing nitrogen and water, and if the combustion is below stoichiometric, oxygen. In the case of ammonia, the nitrogen content is slightly larger and water slightly lower compared to hydrogen. The ammonia laminar flame speed was in the same order as methane, indicating that a similar turbulent flame speed should be expected. The laminar burning velocity of ammonia was 20 and 17 cm/s under the boiler and turbine combustion conditions, respectively. It was found that ammonia had a lower flame temperature compared with other fuels, which affected the heat transfer in both the boiler and the gas turbine. The stochiometric adiabatic flame temperature of ammonia was 2068 K and 2075 K under the boiler and turbine condition, respectively. The maximum level of thermal NO in boiler and turbine was 7.5 and 170 ppm. The maximum fuel NO observed in boiler and turbine was 240 and 280 ppm, respectively. A slightly higher mass input for ammonia combustion in the boiler showed to compensate for its lower heating values for domestic application at the expense of a higher level of NO_X emissions. The highest spatial temperatures and remarkably highest NO_X emissions for ammonia were seen in microgas turbines, compared to other fuels, when the same inlet temperatures were considered. Although the ammonia boiler exhaust's NO_X emissions level was only slightly above the 100 ppm limit, this analysis indicated that appropriate NO_X reduction scenarios need to be adopted to improve ammonia in combustion systems. The NO_X emissions control techniques including high temperature air combustion or flameless may be worthy of further investigation for the deployment of ammonia to the energy grid.

Declaration of competing interest

The authors declare that they have no known competing financial interests or personal relationships that could have appeared to influence the work reported in this paper.

Acknowledgements

Data for this aricle can be accessed through the Cranfield University repository at: https://doi.org/10.17862/cranfield.rd.21429123.v1.

References

[1] B. Bazooyar, A. Ghorbani, A. Shariati, Combustion performance and emissions of petrodiesel and biodiesels based on various vegetable oils in a semi industrial boiler, Fuel 90 (2011) 3078–3092, https://doi.org/10.1016/j.fuel.2011.05.025.
[2] B. Bazooyar, A. Ghorbani, A. Shariati, Physical properties of methyl esters made from alkali-based transesterification and conventional diesel fuel, Energy Sources, Part A Recover. Util. Environ. Eff. 37 (2015) 468–476, https://doi.org/10.1080/15567036.2011.586975.
[3] L. Vinet, A. Zhedanov, A "missing" family of classical orthogonal polynomials, J. Phys. Math. Theor. (2011) 500–507, https://doi.org/10.1088/1751-8113/44/8/085201.
[4] R. Metkemeijer, P. Achard, Ammonia as a feedstock for a hydrogen fuel cell; reformer and fuel cell behaviour, J. Power Sources 49 (1994) 271–282, https://doi.org/10.1016/0378-7753(93)01822-Y.
[5] C. Zamfirescu, I. Dincer, Using ammonia as a sustainable fuel, J. Power Sources 185 (2008) 459–465, https://doi.org/10.1016/j.jpowsour.2008.02.097.
[6] A. Macq, Emploi de l'ammoniac comme combustible de remplacement, Compte Rendu Des Journees d'etudes Sur Les Combust, Carburants Natx. (1941) 286–309.
[7] S.M. Grannell, D.N. Assanis, S.V. Bohac, D.E. Gillespie, The fuel mix limits and efficiency of a stoichiometric, ammonia, and gasoline dual fueled spark ignition engine, J. Eng. Gas Turbines Power 130 (2008), https://doi.org/10.1115/1.2898837.
[8] C. Zamfirescu, I. Dincer, Ammonia as a green fuel and hydrogen source for vehicular applications, Fuel Process, Technol. 90 (2009) 729–737, https://doi.org/10.1016/j.fuproc.2009.02.004.
[9] D. Wang, C. Ji, Z. Wang, S. Wang, T. Zhang, J. Yang, Measurement of oxy-ammonia laminar burning velocity at normal and elevated temperatures, Fuel 279 (2020), https://doi.org/10.1016/j.fuel.2020.118425.
[10] O. Kurata, N. Iki, T. Matsunuma, T. Inoue, T. Tsujimura, H. Furutani, H. Kobayashi, A. Hayakawa, Performances and emission characteristics of NH_3-air and NH_3-CH_4-air combustion gas-turbine power generations, Proc. Combust. Inst. 36 (2017) 3351–3359, https://doi.org/10.1016/j.proci.2016.07.088.
[11] H. Kobayashi, A. Hayakawa, K.D.K.A. Somarathne, E.C. Okafor, Science and technology of ammonia combustion, Proc. Combust. Inst. 37 (2019) 109–133, https://doi.org/10.1016/j.proci.2018.09.029.
[12] K.D.K.A. Somarathne, S. Hatakeyama, A. Hayakawa, H. Kobayashi, Numerical study of a low emission gas turbine like combustor for turbulent ammonia/air premixed swirl flames with a secondary air injection at high pressure, Int. J. Hydrogen Energy 42 (2017) 27388–27399, https://doi.org/10.1016/j.ijhydene.2017.09.089.
[13] T. Honzawa, M. Nishioka, R. Kurose, Numerical study on nitric oxide production of moderate or intense low-oxygen dilution combustion using ammonia and city gas, Heat Tran. Eng. 42 (2021) 1223–1236, https://doi.org/10.1080/01457632.2020.1777016.
[14] J. Choe, W. Sun, T. Ombrello, C. Carter, Plasma assisted ammonia combustion: simultaneous NO_X reduction and flame enhancement, Combust. Flame 228 (2021) 430–432, https://doi.org/10.1016/j.combustflame.2021.02.016.
[15] T. Mendiara, P. Glarborg, Ammonia chemistry in oxy-fuel combustion of methane, Combust. Flame 156 (2009) 1937–1949, https://doi.org/10.1016/j.combustflame.2009.07.006.
[16] M. Ilbas, O. Kumuk, S. Karyeyen, Numerical study of a swirl gas turbine combustor for turbulent air and oxy-combustion of ammonia/kerosene fuels, Fuel (2021) 304, https://doi.org/10.1016/j.fuel.2021.121359.
[17] N.A. Hussein, A. Valera-Medina, A.S. Alsaegh, Ammonia- hydrogen combustion in a swirl burner with reduction of NO_X emissions, Energy Proc. (2019) 2305–2310, https://doi.org/10.1016/j.egypro.2019.01.265.
[18] H. Xiao, A. Valera-Medina, P. Bowen, S. Dooley, 3d simulation of ammonia combustion in a lean premixed swirl burner, Energy Proc. (2017) 1294–1299, https://doi.org/10.1016/j.egypro.2017.12.504.
[19] A. Valera-Medina, S. Morris, J. Runyon, D.G. Pugh, R. Marsh, P. Beasley, T. Hughes, Ammonia, methane and hydrogen for gas turbines, Energy Proc. (2015) 118–123, https://doi.org/10.1016/j.egypro.2015.07.205.
[20] Y. Tang, D. Xie, B. Shi, N. Wang, S. Li, Flammability enhancement of swirling ammonia/air combustion using AC powered gliding arc discharges, Fuel (2021), 122674, https://doi.org/10.1016/j.fuel.2021.122674.
[21] R.C. Rocha, M. Costa, X.S. Bai, Combustion and emission characteristics of ammonia under conditions relevant to modern gas turbines, Combust. Sci. Technol. 193 (2021) 2514–2533, https://doi.org/10.1080/00102202.2020.1748018.
[22] M. Ilbas, O. Kekul, A. Bektas, S. Karyeyen, Oxidizer effects on ammonia combustion using a generated non-premixed burner, Int. J. Hydrogen Energy (2021), https://doi.org/10.1016/j.ijhydene.2021.05.105.
[23] Y. Chen, B. Zhang, Y. Su, C. Sui, J. Zhang, Effect and mechanism of combustion enhancement and emission reduction for non-premixed pure ammonia combustion based on fuel preheating, Fuel 308 (2022), https://doi.org/10.1016/j.fuel.2021.122017.
[24] N. Peters, Laminar flamelet concepts in turbulent combustion, Symp. Combust. 21 (1988) 1231–1250, https://doi.org/10.1016/S0082-0784(88)80355-2.
[25] N. Peters, Laminar diffusion flamelet models in non-premixed turbulent combustion, Prog. Energy Combust. Sci. 10 (1984) 319–339, https://doi.org/10.1016/0360-1285(84)90114-X.
[26] F.R. Menter, Two-equation eddy-viscosity turbulence models for engineering applications, AIAA J. 32 (1994) 1598–1605, https://doi.org/10.2514/3.12149.
[27] B. Bazooyar, H. Gohari Darabkhani, Design, manufacture and test of a micro-turbine renewable energy combustor, Energy Convers. Manag. 213 (2020), 112782, https://doi.org/10.1016/j.enconman.2020.112782.
[28] B. Bazooyar, H. Gohari Darabkhani, The design strategy and testing of an efficient microgas turbine combustor for biogas fuel, Fuel 294 (2021), 120535, https://doi.org/10.1016/j.fuel.2021.120535.
[29] B. Bazooyar, H.G. Darabkhani, Design procedure and performance analysis of a microturbine combustor working on biogas for power generation, Proc. ASME Turbo Expo. 4B-2019 (2019), https://doi.org/10.1115/GT2019-91052.
[30] H. Nakamura, S. Hasegawa, T. Tezuka, Kinetic modeling of ammonia/air weak flames in a micro flow reactor with a controlled temperature profile, Combust. Flame 185 (2017) 16–27, https://doi.org/10.1016/j.combustflame.2017.06.021.
[31] E.W. Kaiser, T.J. Wallington, M.D. Hurley, J. Platz, H.J. Curran, W.J. Pitz, C. K. Westbrook, Experimental and modeling study of premixed atmospheric-pressure dimethyl ether - air flames, J. Phys. Chem. 104 (2000) 8194–8206, https://doi.org/10.1021/jp994074c.
[32] G.P. Smith, D.M. Golden, M. Frenklach, N.W. Moriarty, B. Eiteneer, M. Goldenberg, C.T. Bowman, R.K. Hanson, S. Song, W.C. Gardiner Jr., GRI-mech 3.0, 2012. URL Http//Www. Me. Berkeley. Edu/Gri_mech.
[33] A. Kéromnès, W.K. Metcalfe, K.A. Heufer, N. Donohoe, A.K. Das, C.J. Sung, J. Herzler, C. Naumann, P. Griebel, O. Mathieu, M.C. Krejci, E.L. Petersen, W. J. Pitz, H.J. Curran, An experimental and detailed chemical kinetic modeling study of hydrogen and syngas mixture oxidation at elevated pressures, Combust. Flame 160 (2013) 995–1011, https://doi.org/10.1016/j.combustflame.2013.01.001.
[34] B. Bazooyar, A. Jomekian, A. Shariati, Analysis of the formation and interaction of nitrogen oxides in a rapeseed methyl ester nonpremixed turbulent flame, Energy Fuel. 31 (2017) 8708–8721, https://doi.org/10.1021/acs.energyfuels.7b01278.
[35] Y.B. Zeldovich, 26. Oxidation of nitrogen in combustion and explosions, in: Sel. Work. Yakov Borisovich Zeldovich, I, 2015, pp. 404–410, https://doi.org/10.1515/9781400862979.404.
[36] G.G. De Soete, Overall reaction rates of NO and N_2 formation from fuel nitrogen, Symp. Combust 15 (1975) 1093–1102, https://doi.org/10.1016/S0082-0784(75)80374-2.
[37] N. Selçuk, N. Kayakol, Evaluation of discrete ordinales method for radiative transfer in rectangular furnaces, Int. J. Heat Mass Tran. 40 (1997) 213–222, https://doi.org/10.1016/0017-9310(96)00139-1.
[38] B. Bazooyar, A. Shariati, S.H. Hashemabadi, Turbulent non-premixed combustion of rapeseed methyl ester in a free shear swirl air flow, Ind. Eng. Chem. Res. 55 (2016) 11645–11663, https://doi.org/10.1021/acs.iecr.6b02500.
[39] B. Bazooyar, E. Ebrahimzadeh, A. Jomekian, A. Shariati, NO_X formation of biodiesel in utility power plant boilers. part a: influence of fuel characteristics, Energy Fuel. 28 (2014) 3778–3792, https://doi.org/10.1021/ef500001g.
[40] B. Bazooyar, S.H. Hashemabadi, A. Shariati, NO_X formation of biodiesel in utility power plant boilers; Part B. Comparison of NO between biodiesel and petrodiesel, Fuel 182 (2016) 323–332, https://doi.org/10.1016/j.fuel.2016.05.018.
[41] B. Bazooyar, A. Shariati, S.H. Hashemabadi, Characterization and reduction of NO during the combustion of biodiesel in a semi-industrial boiler, Energy Fuel. 29 (2015) 6804–6814, https://doi.org/10.1021/acs.energyfuels.5b01529.
[42] B. Bazooyar, A. Shariati, M. Khosravi-Nikou, S.H. Hashemabadi, Numerical analysis of nitrogen oxides in turbulent lifted H_2/N_2 cabra jet flame issuing into a vitiated coflow, Int. J. Hydrogen Energy 44 (2019) 13932–13952, https://doi.org/10.1016/j.ijhydene.2019.03.166.
[43] A.J. Reiter, S.C. Kong, Demonstration of compression-ignition engine combustion using ammonia in reducing greenhouse gas emissions, Energy Fuel. 22 (2008) 2963–2971, https://doi.org/10.1021/ef800140f.
[44] J. Li, H. Huang, N. Kobayashi, Z. He, Y. Osaka, T. Zeng, Numerical study on effect of oxygen content in combustion air on ammonia combustion, Energy 93 (2015) 2053–2068, https://doi.org/10.1016/j.energy.2015.10.060.
[45] A. Ghorbani, B. Bazooyar, A. Shariati, S.M. Jokar, H. Ajami, A. Naderi, A comparative study of combustion performance and emission of biodiesel blends and diesel in an experimental boiler, Appl. Energy 88 (2011) 4725–4732, https://doi.org/10.1016/j.apenergy.2011.06.016.
[46] B. Bazooyar, A. Shariati, S.H. Hashemabadi, Economy of a utility boiler power plant fueled with vegetable oil, biodiesel, petrodiesel and their prevalent blends, Sustain. Prod. Consum. 3 (2015) 1–7, https://doi.org/10.1016/j.spc.2015.06.001.
[47] B. Bazooyar, N. Hallajbashi, A. Shariati, A. Ghorbani, An investigation of the effect of input air upon combustion performance and emissions of biodiesel and diesel fuel in an experimental boiler, Energy Sources, Part A Recover. Util. Environ. Eff. 36 (2014) 383–392, https://doi.org/10.1080/15567036.2010.538810.
[48] B. Bazooyar, A. Shariati, A comparison of the emission and thermal capacity of methyl ester of corn oil with diesel in an experimental boiler, Energy Sources, Part A Recover. Util. Environ. Eff. 35 (2013) 1618–1628, https://doi.org/10.1080/15567036.2010.527902.
[49] B. Bazooyar, S.Y. Hosseini, S. Moradi Ghoje Begloo, A. Shariati, S.H. Hashemabadi, F. Shaahmadi, Mixed modified Fe_2O_3-WO_3 as new fuel borne catalyst (FBC) for biodiesel fuel, Energy 149 (2018) 438–453, https://doi.org/10.1016/j.energy.2018.02.062.
[50] E.C. Okafor, K.D.K.A. Somarathne, A. Hayakawa, T. Kudo, O. Kurata, N. Iki, H. Kobayashi, Towards the development of an efficient low-NO_X ammonia

combustor for a micro gas turbine, Proc. Combust. Inst. 37 (2019) 4597–4606, https://doi.org/10.1016/j.proci.2018.07.083.

[51] H.G. Darabkhani, H. Varasteh, B. Bazooyar, Design characteristics of oxyfuel combustor, heat exchanger network and turbomachinery, in: H.G. Darabkhani, H. Varasteh, B.B.T.-C.C.T. for G.-T.-B.P.P. Bazooyar (Eds.), Carbon Capture Technol. Gas-Turbine-Based Power Plants, Elsevier, 2023: pp. 157–181. https://doi.org/10.1016/b978-0-12-818868-2.00004-7.

[52] B. Bazooyar, A. Jomekian, E. Karimi-Sibaki, M. Habibi, H. Gohari Darabkhani, The role of heat recirculation and flame stabilization in the formation of NO_X in a thermo-photovoltaic micro-combustor step wall, Int. J. Hydrogen Energy. 44 (2019) 26012–26027. https://doi.org/10.1016/j.ijhydene.2019.08.061.